Research Article | Vol. 12, No. 5 / 1 May 2022 / Optical Materials Express 2063
Optical Materials EXPRESS

Atomic layer deposition of conformal anti-reflective coatings on complex 3D printed micro-optical systems

SIMON RISTOK, PHILIPP FLAD, AND HARALD GIESSEN*

4th Physics Institute and Research Center SCoPE, University of Stuttgart, Pfaffenwaldring 57, 70569 Stuttgart, Germany
giessen@pi4.uni-stuttgart.de

Abstract: 3D printing of micro-optics has recently become a very powerful fabrication method for sub-millimeter sized optics. Miniature optical systems and entire optical instruments such as endoscopes have become possible with this technique. 3D printed complex micro-optical systems are printed in one single process, rather than being assembled. This precludes anti-reflection coating of the individual lenses before assembly by conventional coating methods such as sputtering or directed plasma etching, as voids between the individual lenses cannot be reached by a directed coating beam. We solve this issue by conformal low-temperature thermal atomic layer deposition (ALD) which is compatible with the low glass transition temperature of the utilized 3D printed polymer materials. Utilizing 4-layer designs, we decrease the broadband reflectivity of coated flat substrates in the visible to below 1%. We characterize and investigate the properties of the coatings based on transmission measurements through coated and uncoated 3D printed test samples as well as through a double-lens imaging system. We find that the reflectivity is significantly reduced and conversely the transmission is enhanced, which is of particular interest for low-light applications. Furthermore, the physical durability and resistance against humidity uptake should also be improved.

1. Introduction

Applications of 3D printed micro-optics have recently emerged in many different fields [1–8], ranging all the way from endoscopic devices for medical purposes [9] over holographic projectors and LED collimators [10,11], achromatic and apochromatic multiplet lenses [12] to scientific topics, e.g., building a miniature spectrometer or an efficient fiber-coupled single photon source [13,14]. 3D printing as manufacturing technique comes with intrinsic advantages for the fabrication of optical elements, namely the possibility to create freeform surfaces such as aspheric lenses as well as the perfect alignment of multi-lens systems fabricated in a single-step process. Like in macroscopic optical systems, there are certain key elements which have to be controlled precisely in order to fabricate a high-quality device. First, the lens material and shape must match the optical design. This is achieved for 3D printed optics by careful characterization of the refractive index and the dispersion of the printing materials and by iterative shape optimization [15,16]. Apart from refractive (or diffractive) lenses, absorptive aperture stops are often implemented in complex optical designs. Those can also be realized for 3D printed micro-optics, e.g., by filling a hollow cavity with an absorptive black liquid or by evaporating absorptive or reflective materials [16,17]. As the number of interfaces in an optical system increases, anti-reflective (AR) coatings become crucial to counteract reflection losses and the formation of ghost images, which reduce the imaging quality. AR coatings on polymer lenses can be deposited by industrial standard processes, e.g., via sputtering for the surface finishing of eyeglasses, or by a variety of nanofabrication techniques, e.g., 3D printing of moth-eye type AR coatings [18], ion-assisted electron beam evaporation [19], or the deposition of thin films

#454475 https://doi.org/10.1364/OME.454475
Journal © 2022 Received 31 Jan 2022; revised 16 Mar 2022; accepted 30 Mar 2022; published 28 Apr 2022

Optical Materials EXPRESS

containing polymer or metal oxide nanoparticles by spin-coating from the liquid phase [20,21]. While those fabrication methods work well on optical elements with a single surface, all of them face certain challenges when more complex 3D printed multi-lens systems with hollow cavities and undercuts need to be coated. Sputtering is a highly directive technique, and for deposition from the liquid phase via spin-coating, the size of the openings on the micrometer scale and surface tension effects can be problematic. Here, a conformal fabrication strategy is required which can deposit the material on every surface in one single step. We achieve this via atomic layer deposition (ALD), using a PICOSUN R-200 Advanced system. Our AR coating consists of four alternating layers of titania (TiO_2) and silica (SiO_2) (Fig. 1(a)). The layer thickness (17 nm TiO_2, 44 nm SiO_2, 27 nm TiO_2, 109 nm SiO_2) has to be tuned precisely to the designed value to ensure minimum reflectivity with target values below 1% between 450 nm and 650 nm. The coating was designed and optimized using the software tool Essential Macleod for a central wavelength of 550 nm and perpendicular incidence. As we use ALD, we strive for a minimum number of thin layers to achieve the design target. Typically, 4% of the incident light are reflected at each interface. As a standard 3D printed free-standing singlet lens has two interfaces, ~8% of light are lost due to reflection (Fig. 1(b)). An AR coating can decrease the total reflection loss down to < 1% for the main part of the visible wavelength spectrum. For a singlet lens, both surfaces can in principle be coated successively. This way, coating techniques like electron beam assisted evaporation [22] or ion-assisted plasma etching can be used [23]. More complex 3D printed multi-lens systems often contain undercuts and cavities, therefore different coating techniques are required.

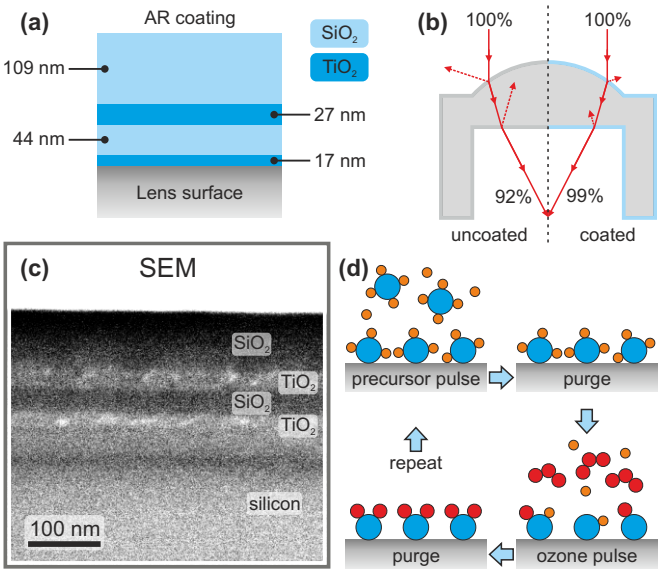

Fig. 1. (a) AR coating design. (b) Illustration of transmission through uncoated and AR coated lens. (c) Scanning electron microscopy image of a cleaving face of a coated silicon reference wafer. (d) Atomic layer deposition cycle.

2. Fabrication

We investigate low-temperature (150 °C) thermal atomic layer deposition, which enables the simultaneous coating of all external and internal surfaces of an optical lens system in one single step without inflicting thermal damage on the polymer structures. The glass transition temperature of the polymeric lens material is in the range above 200 °C, which is much higher

Optical Materials EXPRESS

than the temperatures in our ALD reactor. ALD as multilayer coating process on glass and polymer materials has been successfully demonstrated in the past [24–27]. Also, it was shown that ALD-deposited high-reflectance coatings worked in silicon substrate tubes and wedges [28]. Apart from the optical anti-reflective property, the inorganic coatings also increase the physical and chemical durability of 3D printed polymer structures, which is in particular important for medical endoscopic applications, where resistance against humidity is required [29]. The different materials are deposited in successive process cycles, each consisting of four steps illustrated in Fig. 1(d). First, precursor molecules containing silicon (Si) or titanium (Ti) form a thin self-terminated layer on the lens surface and the excess molecules are purged. As precursors, we used Hexakis(ethylamino)disilane and Tetrakis(dimethylamido)titanium(IV), which were available as thermal low-temperature ALD process materials for our PICOSUN machine. The organic parts of the precursor molecules are then replaced by oxygen provided by ozone molecules. After the reaction byproducts have been purged, a single layer of TiO_2 or SiO_2 has formed on the lens surface. The thickness of such a layer is typically in the range of 0.1 nm, and by carefully tuning the number of deposition cycles the overall layer thickness can be adjusted very precisely. The total deposition time for the AR coating described here is ~14 h. The refractive indices and the thickness of reference layers on silicon were measured using angle-dependent ellipsometry (J.A. Woolam Co. RC2) during process development. This also assured proper film stoichiometry.

During the fabrication, the formation of thin cracks in the AR coating on 3D printed structures could sometimes be observed. We attribute this to internal tension caused by the different thermal expansion properties of the inorganic coating material and the underlying polymer. First experiments indicate that this can be counteracted by either avoiding sharp angled edges (to reduce possible starting locations for cracks) or by adding a thin (~5 nm) adhesion layer of ALD-deposited alumina (Al_2O_3) between polymer and the actual AR coating [24]. The influence of the additional alumina layer on the optical properties of the entire layer stack is negligible as the layer is comparably thin, which is also supported by simulations. Recent experiments have shown that 1.5 nm Al_2O_3 prevent cracks as well.

We use scanning electron microscopy (SEM) to analyze the fabricated layer structure. The different layers are clearly visible in the SEM image in Fig. 1(c), where the cleaving face of a coated silicon wafer is depicted. Contrast enhancement was applied for better visibility. The silicon wafer is used as reference substrate for ellipsometric layer characterization to calibrate the ALD process.

3. Reflectivity measurements

For a quantitative characterization of our coatings we perform reflectivity measurements, using a Cary 7000 spectrophotometer. First, we compare an uncoated 1×1 cm^2 glass substrate to substrates with one and two coated surfaces (Fig. 2(a)). In the inset, a visual comparison of coated and uncoated substrates is shown. The different appearance of a bright-to-dark transition illustrates the different reflective properties of the substrates. This is confirmed by the reflectivity measurements, where the uncoated glass has a reflectivity of ~8-9% between 400 nm and 800 nm (black), as reflected light from the front and the back of the substrate is collected. The reflectivity at 550 nm is significantly reduced when we apply an AR coating to one side of the substrate (blue). When both sides are coated, the reflectivity is further reduced to $< 1\%$ between ~450 nm and ~680 nm, covering the main part of the visible wavelength spectrum. As we measure the reflection from both sides of the substrate, the reflectivity of a single AR coated interface is less than 0.5% across that spectral range. The next step towards an AR coated 3D printed lens system is the characterization of an AR coating on a flat 3D printed structure. We use a Nanoscribe Quantum X microfabrication system to print a plate of 30 µm thickness and an area of $\sim 6 \times 6$ mm^2 onto a glass substrate (inset in Fig. 2(b)). The writing objective has a magnification of

Optical Materials EXPRESS

25x and the resist is Nanoscribe IP-S. Because such large and thin structures have the tendency to delaminate from the supporting substrate due to internal tensions induced by shrinking, the structure consists of individual 500×500 µm^2 plates which are separated by gaps of 7 µm. This is sufficient to ensure good adhesion to the glass surface while the gaps are small enough to have negligible influence on the reflectivity measurements. AR coatings are deposited on the printed structure and on the back of the supporting glass substrate. Compared to the bare glass substrate in Fig. 2(a), the reflectivity of the uncoated structure (black) in Fig. 2(b) is slightly lower in general. This could originate from absorption inside the 3D printed plate and scattering at the surface or inside the plate. Furthermore, the reflectivity decreases rapidly for wavelengths < 420 nm. This is caused by absorption and scattering inside the printed plate, as the resist is designed to be hardened by UV light at 390 nm. The two-sided coated sample has a reflectivity < 1% between ~420 nm and ~640 nm, demonstrating the compatibility of our coating design and process with both glass and polymer surfaces.

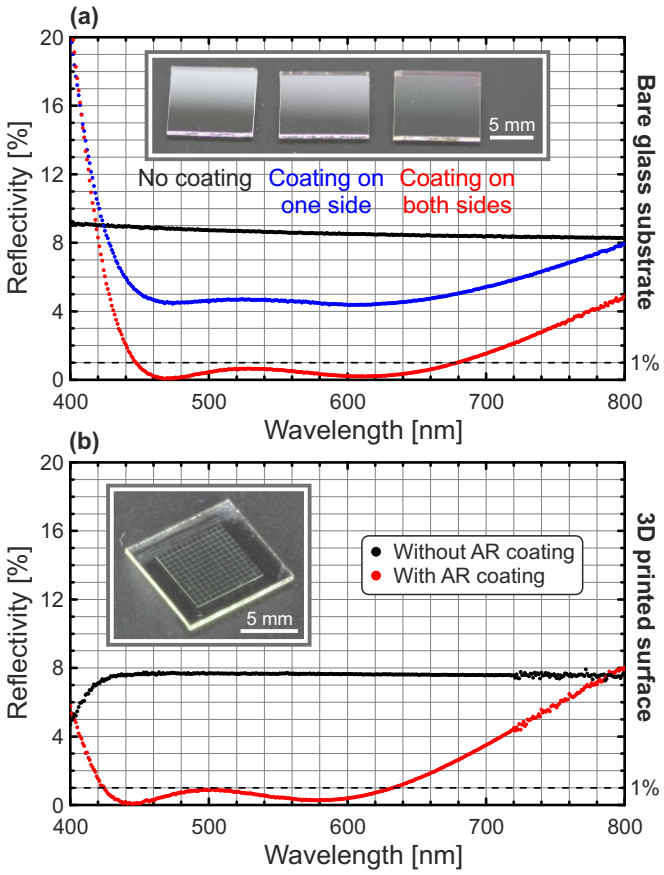

Fig. 2. AR coatings on flat substrates. (a) Reflectivity measurements of an uncoated glass substrate and substrates with one and two AR coated surfaces. Light reflected from both front and back of substrate is measured. A visual comparison of coated and uncoated substrates is shown in the inset. (b) Reflectivity of coated and uncoated 3D printed flat structure shown in the inset. The coating is on both sides of the sample.

Optical Materials EXPRESS

4. Transmission experiments

While the coated structures discussed so far have only two reflecting surfaces, the importance of AR coatings increases significantly for systems with more optical interfaces. To illustrate this,

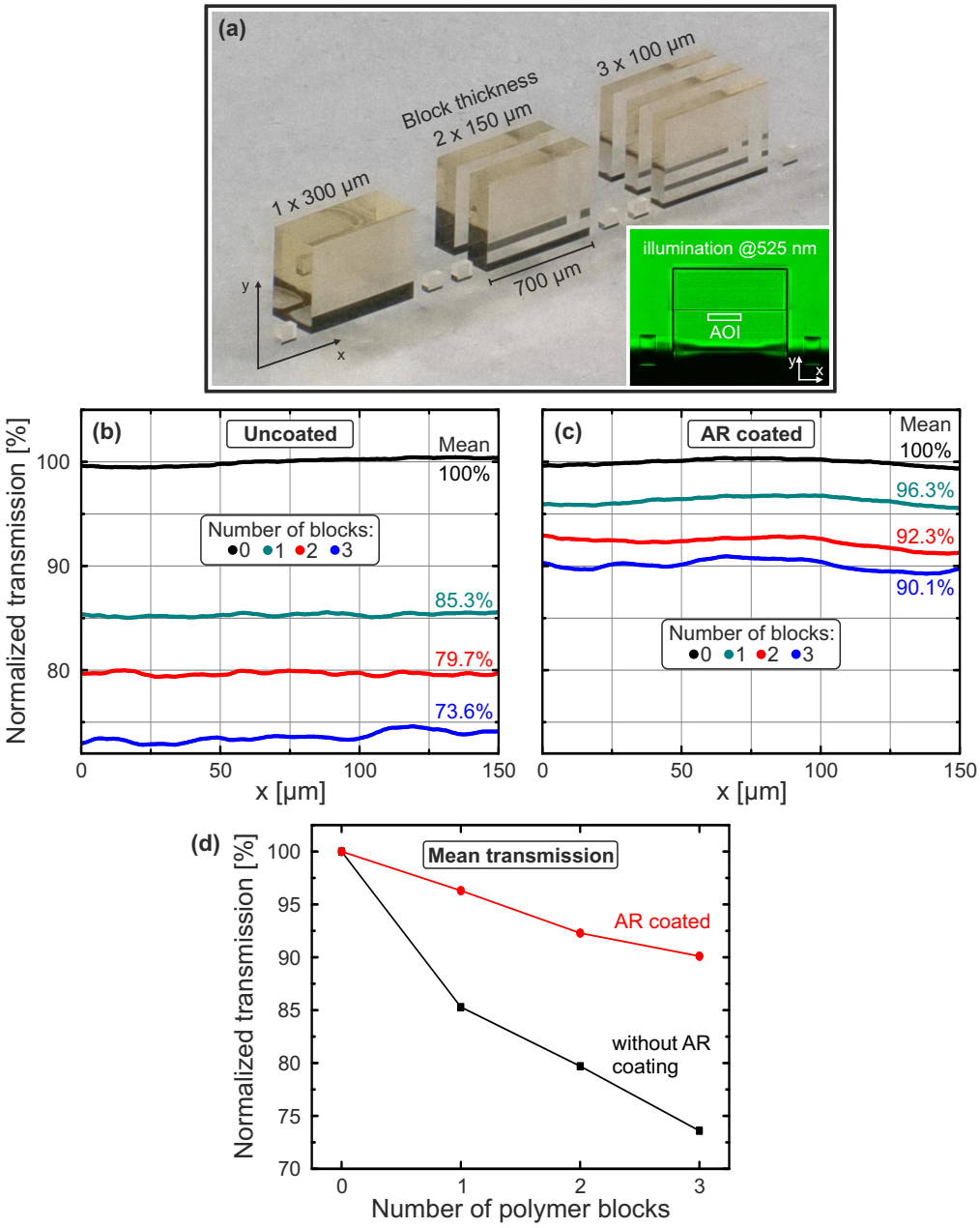

Fig. 3. Transmission test sample. (a) 3D printed polymer block sets with identical overall thickness. Inset shows an image of the sample with transmitted light at 525 nm. The rectangle indicates the area of interest (AOI) from which transmission data was extracted. (b) and (c) Normalized transmission through different numbers of uncoated and AR coated polymer blocks at 525 nm. The x axis runs along the longest edge of the polymer blocks. (d) Mean transmission of AR coated and uncoated polymer blocks.

Optical Materials EXPRESS

we measure the transmission through polymer blocks of different size (Fig. 3(a)). The blocks are 520 µm high and 700 µm wide. The biggest block has a thickness of 300 µm, the two blocks are 150 µm thick and the three blocks are 100 µm in thickness. Light traveling through the different block sets should thus experience the same amount of absorption inside the 3D printed structures, therefore a reduced transmission can be attributed exclusively to reflection losses. The small blocks left and right of the big blocks are printed to facilitate focusing, ensuring an equal focal position for all measurements. The inset shows a front view of an AR coated block (thickness: 300 µm) under illumination at 525 nm, the wavelength of our LED illumination. The horizontal line indicates the boundary between the lower and the upper half of the block, which are printed successively, due to the limited working distance of the printing objective. The rectangle indicates the area of interest (AOI) from which the transmission curves in Fig. 3(c) are extracted. We calculate the mean intensity for each pixel column in y direction and apply a moving average to generate the transmission profiles along the x axis. In Fig. 3(b) the normalized transmission through different uncoated block sets is shown. The black data points represent a measurement without any 3D printed structure and the mean value is set to 100%, serving as reference. The transmission through the block structures is reduced by reflections at the two interfaces of each block, resulting in 85.3% transmission for the single block, 79.7% for the set of two blocks and 73.6% for the set of three blocks. In comparison, the transmission through coated blocks in Fig. 3(c) is 96.3%, 92.3% and 90.1% respectively, clearly emphasizing the performance of our AR coatings. The mean transmission of the AR coated and uncoated polymer blocks are summarized and compared in Fig. 3(d).

5. Doublet lens with AR coating

Finally, we combine our AR coating with a double-lens imaging design depicted in Fig. 4(a). The first smaller lens is printed directly on a glass substrate with 500 µm thickness. The backside of the substrate was AR coated prior to the 3D printing step. The bigger second lens is connected to the substrate via supporting structures visible in the microscope image in Fig. 4(b), which also emphasizes the advantage of our non-directional coating process: the space between the two lenses and thus the surface of lens 1 and the lower surface of lens 2 cannot be coated using conventional directional coating techniques. The large openings in the supporting structure should facilitate gas distribution during the ALD process, resulting in a homogeneous coating on all surfaces. Both lenses are printed utilizing the grayscale writing mode of our Nanoscribe Quantum X microfabrication system, resulting in optically smooth surface quality. The root mean square roughness (ISO 25178) of the bigger lens was determined to be Sq ≈ 15 nm without AR coating. After the coating process, the roughness was reduced even further to Sq ≈ 9 nm.

We compare images of a 1951 USAF resolution test target viewed by an uncoated and an AR coated doublet lens (Fig. 4(c) and (d)). The illumination setup consist of a white-light LED source, a collimation lens, a diffuser plate and a focusing objective. To simulate the aperture stop from the optical design, we add an adjustable iris diaphragm which is imaged onto the printed lens. The microscopy setup is described in detail in [30]. For both images identical illumination conditions were used. The overall imaging quality is very similar, but when looking at the bright square between element 2 of group 0 and element 1 of group 1, it is apparent that the coated lens transmits more light. For a quantitative analysis, we compare intensity profiles extracted along the red line through element 1 of group 0. The black curve in Fig. 4(e) represents the uncoated lens and the red curve is associated with the AR coated lens. It is obvious that the overall intensity transmitted through the coated lens is higher. When we multiply the black curve by a factor of 1.2, the result (black dotted line) is in good agreement with the red curve, indicating a transmission increase of ~20%. This is a significant improvement when short exposure times are required, especially for low-light applications.

Optical Materials EXPRESS

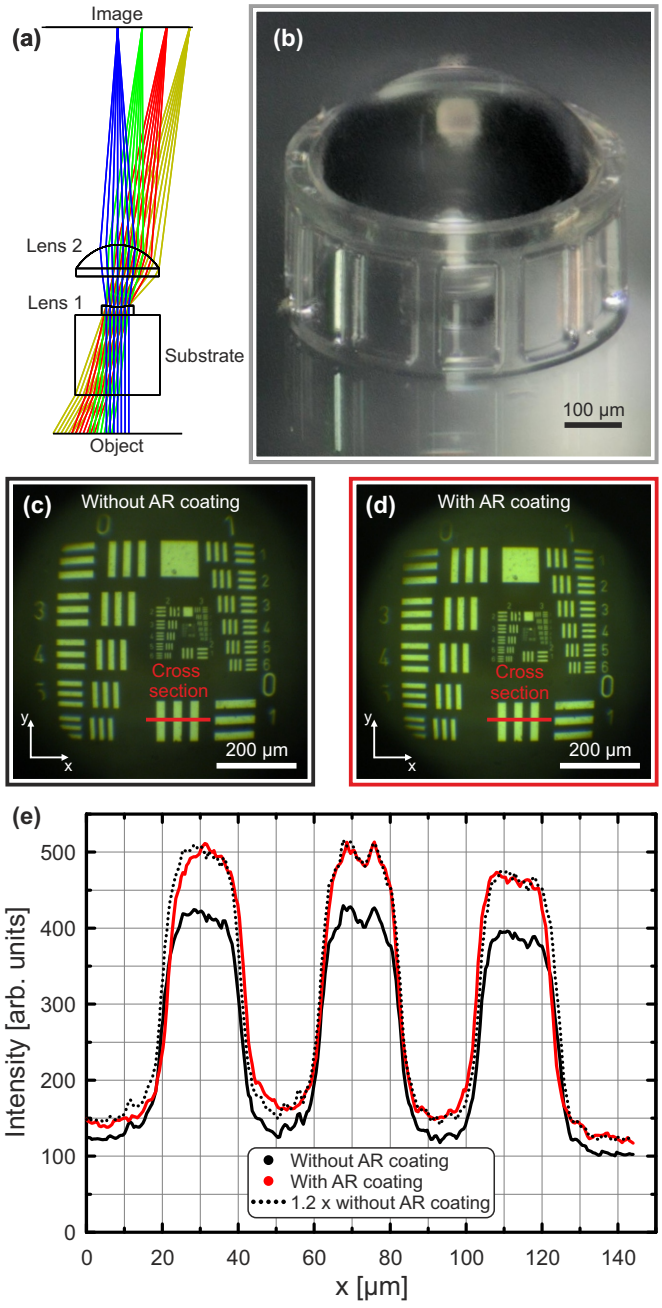

Fig. 4. Double-lens imaging system. (a) Optical design. (b) Microscope image of lens system with supporting structures. (c) and (d) USAF 1951 resolution test target imaged by an uncoated and an AR coated lens system. (e) Intensity profiles extracted from (c) and (d).

Optical Materials EXPRESS

It might be intuitive to also expect an increased imaging contrast for the coated lens, as more light is transmitted. For objects with periodic geometry such as the 1951 USAF target, the definition of the Michelson contrast

$$\frac{I_{max} - I_{min}}{I_{max} + I_{min}} \tag{1}$$

is usually used to quantify the modulation between bright and dark regions [31]. Here, I_{max} and I_{min} are the intensities at the peaks and at the two internal minima of the profiles. As our AR coating simply leads to an overall increase in transmission, both I_{max} and I_{min} are multiplied with the same factor, which effectively does not change the contrast at all.

6. Conclusion

We have demonstrated the fabrication of anti-reflective coatings on 3D printed polymer optics by atomic layer deposition. This conformal coating process enables the single-step formation of AR coatings on every surface of a complex micro-optical system, including undercuts and hollow cavities. The coatings can reduce reflection from standard glass substrates and 3D printed flat structures to below 1% for the main part of the visible wavelength spectrum. Transmission measurements of different 3D printed test structures were performed. Here, the transmission through six interfaces was increased from ~74% to ~90% by the AR coating. Finally, a resolution test target viewed by a 3D printed double-lens imaging system exhibits ~20% more overall intensity compared to an uncoated lens. This is in particular interesting for applications where the amount of accessible illumination light or the exposure time of a camera sensor is limited. In the future, we will combine our AR coatings with more complex optical systems, consisting of more than two lenses. Here, we will make use of advanced coating designs with more layers, resulting in even lower reflection losses for designated wavelengths. Apart from AR coatings, thin film systems with other optical properties, e.g., chromatic filters, can also be included directly in 3D printed micro-optics by our ALD process.

Funding. Bundesministerium für Bildung und Forschung (03EGSBW575); H2020 European Research Council (862549); Ministerium für Wissenschaft, Forschung und Kunst Baden-Württemberg (Innovation Campus Future Mobility); Baden-Württemberg Stiftung (OPTERIAL); Deutsche Forschungsgemeinschaft (DFG-UP31/1).

Acknowledgments. We thank Mario Hentschel for help with SEM images and Moritz Flöss for help with photography. This publication was supported by the Open Access Publishing Fund of the University of Stuttgart.

Disclosures. The authors declare that there are no conflicts of interest related to this article.

Data availability. Data underlying the results presented in this paper are not publicly available at this time but may be obtained from the authors upon reasonable request.

References

1. S. Woska, A. Münchinger, D. Beutel, E. Blasco, J. Hessenauer, O. Karayel, P. Rietz, S. Pfleging, R. Oberle, C. Rockstuhl, M. Wegener, and H. Kalt, "Tunable photonic devices by 3D laser printing of liquid crystal elastomers," Opt. Mater. Express **10**(11), 2928 (2020).
2. A. Landowski, J. Gutsche, S. Guckenbiehl, M. Schönberg, G. Von Freymann, and A. Widera, "Coherent remote control of quantum emitters embedded in polymer waveguides," APL Photonics **5**(1), 016101 (2020).
3. M. Blaicher, M. R. Billah, J. Kemal, T. Hoose, P. Marin-Palomo, A. Hofmann, Y. Kutuvantavida, C. Kieninger, P. I. Dietrich, M. Lauermann, S. Wolf, U. Troppenz, M. Moehrle, F. Merget, S. Skacel, J. Witzens, S. Randel, W. Freude, and C. Koos, "Hybrid multi-chip assembly of optical communication engines by in situ 3D nano-lithography," Light: Sci Appl **9**(1), 71 (2020).
4. L. Jonušauskas, D. Gailevičius, S. Rekštytė, T. Baldacchini, S. Juodkazis, and M. Malinauskas, "Mesoscale laser 3D printing," Opt. Express **27**(11), 15205 (2019).
5. X. Q. Liu, R. Cheng, J. X. Zheng, S. N. Yang, B. X. Wang, B. F. Bai, Q. D. Chen, and H. B. Sun, "Wear-resistant blazed gratings fabricated by etching-assisted femtosecond laser lithography," J. Lightwave Technol. **39**(14), 4690–4694 (2021).
6. V. Melissinaki, O. Tsilipakos, M. Kafesaki, M. Farsari, and S. Pissadakis, "Micro-ring resonator devices prototyped on optical fiber tapers by multi-photon lithography," IEEE J. Sel. Top. Quantum Electron. **27**(6), 1–7 (2021).

Optical Materials EXPRESS

7. G. S. Sokolovskii, V. Melissinaki, K. A. Fedorova, V. V. Dudelev, S. N. Losev, V. E. Bougrov, W. Sibbett, M. Farsari, and E. U. Rafailov, "3D laser nano-printing on fibre paves the way for super-focusing of multimode laser radiation," Sci. Rep. **8**(1), 14618–9 (2018).
8. A. Bertoncini and C. Liberale, "3D printed waveguides based on photonic crystal fiber designs for complex fiber-end photonic devices," Optica **7**(11), 1487 (2020).
9. J. Li, S. Thiele, B. C. Quirk, R. W. Kirk, J. W. Verjans, E. Akers, C. A. Bursill, S. J. Nicholls, A. M. Herkommer, H. Giessen, and R. A. McLaughlin, "Ultrathin monolithic 3D printed optical coherence tomography endoscopy for preclinical and clinical use," Light: Sci Appl **9**(1), 124 (2020).
10. S. Schmidt, S. Thiele, A. Toulouse, C. Bösel, T. Tiess, A. Herkommer, H. Gross, and H. Giessen, "Tailored micro-optical freeform holograms for integrated complex beam shaping," Optica **7**(10), 1279 (2020).
11. S. Thiele, T. Gissibl, H. Giessen, and A. M. Herkommer, "Ultra-compact on-chip LED collimation optics by 3D femtosecond direct laser writing," Opt. Lett. **41**(13), 3029 (2016).
12. M. Schmid, F. Sterl, S. Thiele, A. Herkommer, and H. Giessen, "3D printed hybrid refractive/diffractive achromat and apochromat for the visible wavelength range," Opt. Lett. **46**(10), 2485–2488 (2021).
13. A. Toulouse, J. Drozella, S. Thiele, H. Giessen, and A. Herkommer, "3D-printed miniature spectrometer for the visible range with a 100×100 μm^2 footprint," Light Adv. Manuf. **2**(1), 20 (2021).
14. L. Bremer, K. Weber, S. Fischbach, S. Thiele, M. Schmidt, A. Kaganskiy, S. Rodt, A. Herkommer, M. Sartison, S. L. Portalupi, P. Michler, H. Giessen, and S. Reitzenstein, "Quantum dot single-photon emission coupled into single-mode fibers with 3D printed micro-objectives," APL Photonics **5**(10), 106101 (2020).
15. M. Schmid, D. Ludescher, and H. Giessen, "Optical properties of photoresists for femtosecond 3D printing: refractive index, extinction, luminescence-dose dependence, aging, heat treatment and comparison between 1-photon and 2-photon exposure," Opt. Mater. Express **9**(12), 4564 (2019).
16. K. Weber, Z. Wang, S. Thiele, A. Herkommer, and H. Giessen, "Distortion-free multi-element Hypergon wide-angle micro-objective obtained by femtosecond 3D printing," Opt. Lett. **45**(10), 2784 (2020).
17. A. Toulouse, S. Thiele, H. Giessen, and A. M. Herkommer, "Alignment-free integration of apertures and nontransparent hulls into 3D-printed micro-optics," Opt. Lett. **43**(21), 5283 (2018).
18. Y. Li, D. B. Fullager, E. Angelbello, D. Childers, G. Boreman, and T. Hofmann, "Broadband near-infrared antireflection coatings fabricated by three-dimensional direct laser writing," Opt. Lett. **43**(2), 239 (2018).
19. J. Canning, C. Clark, M. Dayao, D. De Lamela, M. Logozzo, and J. Zhao, "Anti-reflection coatings on 3D-printed components," Coatings **11**(12), 1519 (2021).
20. H. Jiang, W. Zhao, C. Li, and Y. Wang, "Polymer nanoparticle-based porous antireflective coating on flexible plastic substrate," Polymer **52**(3), 778–785 (2011).
21. K. C. Krogman, T. Druffel, and M. K. Sunkara, "Anti-reflective optical coatings incorporating nanoparticles," Nanotechnology **16**(7), S338–S343 (2005).
22. R. Shakoury and R. R. Willey, "Ion assisted deposition of magnesium fluoride films at low temperature," Opt. Quantum Electron. **50**(8), 322 (2018).
23. A. Kaless, U. Schulz, P. Munzert, and N. Kaiser, "NANO-motheye antireflection pattern by plasma treatment of polymers," Surf. Coatings Technol. **200**(1-4), 58–61 (2005).
24. P. Paul, K. Pfeiffer, and A. Szeghalmi, "Antireflection coating on PMMA substrates by atomic layer deposition," Coatings **10**(1), 64 (2020).
25. K. Pfeiffer, L. Ghazaryan, U. Schulz, and A. Szeghalmi, "Wide-angle broadband antireflection coatings prepared by atomic layer deposition," ACS Appl. Mater. Interfaces **11**(24), 21887–21894 (2019).
26. K. Pfeiffer, U. Schulz, A. Tünnermann, and A. Szeghalmi, "Antireflection coatings for strongly curved glass lenses by atomic layer deposition," Coatings **7**(8), 118 (2017).
27. A. Szeghalmi, M. Helgert, R. Brunner, F. Heyroth, U. Gösele, and M. Knez, "Atomic layer deposition of Al_2O_3 and TiO_2 multilayers for applications as bandpass filters and antireflection coatings," Appl. Opt. **48**(9), 1727–1732 (2009).
28. N. T. Gabriel and J. J. Talghader, "Optical coatings in microscale channels by atomic layer deposition," Appl. Opt. **49**(8), 1242–1248 (2010).
29. L. Patsiouras, E. Skotadis, N. Gialama, C. Drivas, S. Kennou, K. Giannakopoulos, and D. Tsoukalas, "Atomic layer deposited Al_2O_3 thin films as humidity barrier coatings for nanoparticle-based strain sensors," Nanotechnology **29**(46), 465706 (2018).
30. S. Ristok, S. Thiele, A. Toulouse, A. M. Herkommer, and H. Giessen, "Stitching-free 3D printing of millimeter-sized highly transparent spherical and aspherical optical components," Opt. Mater. Express **10**(10), 2370 (2020).
31. A. A. Michelson, *Studies in Optics* (The University of Chicago Press, 1927).